ELSEVIER

Thermochimica Acta 396 (2003) 87–96

thermochimica acta

www.elsevier.com/locate/tca

Structure and properties of melt-spun high acrylonitrile copolymer fibers via continuous zone-drawing and zone-annealing processes

Zongquan Wu [a], Anqiu Zhang [a], Simona Percec [b], Shi Jin [a], Alexander J. Jing [a], Jason J. Ge [a], Stephen Z.D. Cheng [a,*]

[a] *Department of Polymer Science, The Maurice Morton Institute, The University of Akron, Akron, OH 44325-3909, USA*
[b] *BP/Amoco Chemicals, Research and Development, Naperville, IL 60563, USA*

Received 31 December 2001; received in revised form 26 July 2002; accepted 2 October 2002

On the occasion of 70th birthday of Professor B. Wunderlich, for his life and pioneering contributions in teaching and researches of polymer physical chemistry and thermal science

Abstract

Continuous zone-drawing and zone-annealing processes have been utilized to probe improvements in mechanical performance of melt-spun high acrylonitrile copolymer fibers (AMLON^{TM}). The as-spun fibers were zone-drawn at different ratios in a narrow temperature range of 100–105 °C and then zone-annealed. As a result of these processes, the fibers show substantial increases in tensile strength and tensile modulus (about three times) and significant improvements in elongation-at-break (about two times) after zone annealing. The thermal transition behavior, dimensional stability and dynamic relaxation properties of the as-spun, zone-drawn and zone-annealed fibers have been studied using differential scanning calorimetry, thermal mechanical and dynamic mechanical experiments. Their mechanical and thermal property changes after the zone-drawing and zone-annealing processes can be associated with the microscopic structural evolution including crystallinity, crystal orientation and apparent crystallite size detected by wide angle X-ray diffraction experiments.

Keywords: Polyacrylonitrile and copolymers; Melt-spun fibers; Structure–property relationships

1. Introduction

Many studies have been carried out on the development of melt-spun polyacrylonitrile fibers using water or solvent as plasticizer [1,2], or using copolymerization of acrylonitrile and acetonitrile [3]. Recently, a family of acrylic resins that can be conventionally melt-spun into fibers (having the trade name of AMLON^{TM}) has been developed at BP/Amoco Chemical Company. These resins have an enhanced compositional uniformity that enables them to survive rigors of the melt spinning processes. The characteristic values of the tensile modulus and tensile strength of the as-spun fibers can reach 4 and 0.1 GPa, respectively.

The physical characteristics of fibers are normally altered and improved by changing processing parameters. For example, since 1980s the zone-drawing and zone-annealing processes have been proposed and applied to various fibers including poly(ethylene terephthalate) (PET) [4], isotactic polypropylene [5,6], nylon 6 and nylon 6,6 [7–9]. In these approaches, an Instron instrument was used to carry out the zone-drawing and zone-annealing processes and thus these processes

* Corresponding author.
E-mail address: scheng@uakron.edu (S.Z.D. Cheng).

0040-6031/02/$ – see front matter
PII: S0040-6031(02)00529-4

were not continuously operated. Recently, continuous zone-drawing and zone-annealing processes have been successfully designed and applied in developing a series of aromatic polyimide fibers [10–12]. After these fibers were zone drawing, their tensile moduli and tensile strengths have increased to 100 and 3 GPa, respectively. In a recent report, the continuous zone-drawing and zone-annealing processes have also been applied to PET fibers [13].

In this study, results on using the continuous zone-drawing and zone-annealing processes to improve the mechanical performance of AMLON™ fibers are presented. Different zone-drawing/annealing conditions have been designed to monitor changes in the mechanical and thermal properties. It is found that these macroscopic property changes are critically associated with the microscopic structural evolutions in the fibers.

2. Experimental

2.1. Resins and fibers

AMLON™ resin was synthesized at BP/Amoco Chemicals and the detailed synthetic route was reported previously [14]. Using controlled polymerization techniques, sequentially ordered copolymers were produced, and the resulting copolymers were more thermally stable and melt processable. The resin was spun into fibers using traditional extruder/spinnerette systems and three fiber samples were supplied for this study: as-spun and two drawn fibers (FS22 and FS16). The latter two fibers were produced from the as-spun fibers, which were subjected to different drawing conditions.

Equipment and experiments. A schematic diagram of the continuous zone-drawing and zone-annealing apparatus used in this study is given in Fig. 1. The apparatus consisted of tension controller, supply and winding spools, temperature controlled zone heater and, speed control motors. The as-spun fibers were passed from the supply spool through the temperature controlled zone heater, the guide and finally wounded on the winding spool. The supply and winding spools were attached to speed control motors. During continuous zone-drawing, the speed of the winding spool was maintained at a higher level than that of the supply spool. As-spun fibers were passed through the zone heater at 100–105 °C with a drawing ratio between three and seven times. During the zone-annealing, the speed of winding spool was maintained at the same level as that of the supply spool and, therefore, it was equivalent to the annealing process of fixed fiber lengths. The zone-drawn fibers were annealed by passing through the heated zone and the temperature was controlled in a narrow window between 140 and 150 °C. The speed of the fibers for this annealing was at 200 mm/min.

Mechanical property measurements including tensile strength, tensile modulus and elongation-at-break were carried out on an Instron model 1130. The gage length was 250 mm and a speed of 10 cm/min was

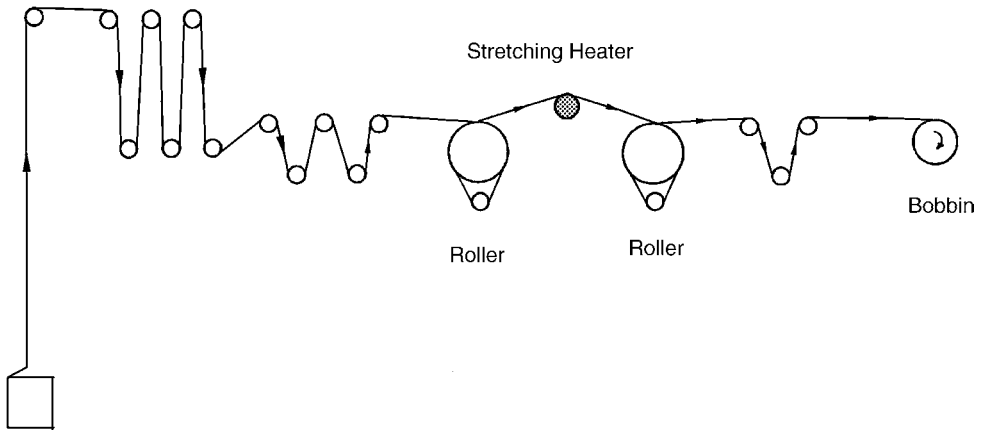

Fig. 1. Schematic representation of apparatus for continuous zone-drawing and zone-annealing processes.

applied to obtain stress–strain curves. These tensile strength, tensile modulus and elongation-at-break were obtained from the stress–strain relationships.

Wide angle X-ray diffraction (WAXD) measurements were conducted using a Rigaku RAXIS-IV image plate with an 18 kW X-ray generator and a monochromator. The X-ray crystallinity determination of the fibers was generated by the subtraction of the background and amorphous scattering halo generated by the amorphous fiber WAXD pattern. The 2θ range was between 3° and 40°. The reflection peak positions and widths observed were calibrated using silicon crystals of known crystal sizes in the high-angle region ($2\theta > 15°$) and silver behenate in the low-angle region ($2\theta < 15°$).

The crystal orientation in the fiber was calculated using the Herman's equation:

$$f_c \times 100\% = \frac{1}{2}\left(3\left\langle\cos^2\phi\right\rangle - 1\right) \quad (1)$$

where f_c is the orientation factor along the fiber direction and ϕ the angle between the fiber axis and the c-axis of the crystal unit cell. Since AMLON^{TM} fibers exhibited a pseudo-hexagonal packing in two-dimensional ordered array, it is difficult to find the (0 0 l) diffraction, the (1 1 0) crystallographic plane was used to calculate the degree of crystal orientation.

The numerical values for the mean square cosine in Eq. (1) were determined from the fully corrected azimuthal intensity distribution diffracted from the (1 1 0) crystallographic plane using the following equation:

$$\cos^2\phi = \frac{\int I(\cos^2\phi)(\sin\phi)\,\mathrm{d}\phi}{\int I(\sin\phi)\,\mathrm{d}\phi} \quad (2)$$

The determination of the apparent crystallite size in the fibers perpendicular to the (1 1 0) planes was conducted by using the Scherrer equation:

$$L = \frac{K\lambda}{(\beta^2 - b^2)^{1/2}} \quad (3)$$

where β and b are, respectively, the width at half maximum of the (1 1 0) plane diffraction and the instrumental broadening factor ($b = 0.3$, which was determined by equipment calibration), and K a geometry dependent constant that was assumed to be unity.

Differential scanning calorimetry (DSC) measurements were carried out on a thermal analyzer TA 2920. The DSC scans were performed within the temperature range of 25–300 °C at a heating rate of 10 °C/min. All measurements were carried out under nitrogen flow (40 ml/min). The temperature and heat of fusion scales of this DSC were calibrated using the standard materials. The thermal shrinkage and shrinkage force of the fibers were measured on a Seiko stress–strain thermal mechanical analyzer (TMA/SS 100) in a temperature range of 25–220 °C using a heating rate of 10 °C/min. A bundle of fibers (250 d) was clamped into the sample holder with a small initial stress in order to keep the fibers straight. The changes of stress at constant length were determined within this temperature range using a heating rate of 10 °C/min. Thermal dynamic mechanical measurements were conducted on a Seiko DMA 200 using a bundle of fibers (250 d) clamped into the sample holder with a small initial stress. The frequency applied was between 0.1 and 10 Hz over a temperature range of 25–220 °C. The storage moduli (E') and loss moduli (E'') were measured and the loss factor $\tan\delta$ was derived from the ratio between E'' and E'.

3. Results and discussion

3.1. Optimal conditions for the continuous zone-drawing and zone-annealing

The as-spun AMLON^{TM} fibers were zone-drawn and then zone-annealed to probe the improvement in fiber mechanical properties. The zone drawing was carried out above the glass transition temperature of the fibers ($T_g = 85$ °C, see below). Preliminary drawing experiments were performed over a temperature range of 90–110 °C. A narrow temperature window of 100–105 °C has been found to be optimized in generating high draw ratios in the fibers. Fig. 2 and Table 1

Table 1
The mechanical properties of AMLON^{TM} fibers with different draw ratio (at drawing temperatures between 100 and 105 °C)

Draw ratio	Tensile strength	Elongation-at-break (%)	Modulus
0	0.10	45	4.1
2.1	0.23	19	6.2
3.4	0.30	11	9.0
4.6	0.34	9.4	10.5
5.5	0.32	7.5	11.2
7.2	0.29	5.2	12.4

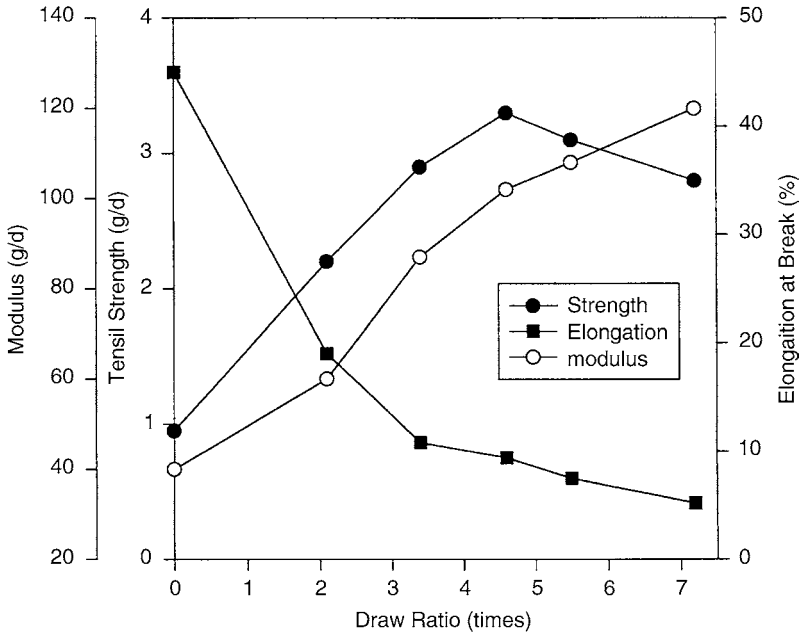

Fig. 2. The mechanical properties of the fibers with different draw ratio (at drawing temperatures between 100 and 105 °C).

show the tensile properties of the AMLON™ fibers drawn at different ratios in this temperature window. It is evident that the tensile strengths of the fibers initially increase with increasing the draw ratio, and the best tensile strength can be achieved when the fiber is drawn to a ratio of 4–5. Increasing the draw ratio exceeding five times results in a minor decrease of the fiber tensile strength. It can also be observed that with increasing the draw ratio, the elongation-at-break gradually decreases, while the modulus of the fibers is enhanced. Since the zone-drawing optimal condition is determined by the tensile mechanical properties achieved, the fiber drawn ratios of 4–5 times are selected for further zone-annealing experiments. Compared with the as-spun fiber, the tensile modulus and tensile strength of the zone-drawn fibers are three times higher. The tensile modulus and tensile strength of the zone-drawn fibers can reach 10 and 0.3 GPa, respectively, while the elongation-at-break decreases to about 11% of the original value obtained in as-spun fibers (45%).

For the zone-annealing experiments, the starting conditions can be chosen based on the mechanical performance of the oven-annealed fiber samples although these conditions may vary when applied to the continuous zone-annealing process. Based on the results obtained from the oven-annealed fibers, the continuous zone-annealing experiments were carried out in a temperature range of 130–150 °C at an annealing speed of 150–300 mm/min. The optimal conditions are found in a zone-annealing temperature window of 140–150 °C at an annealing speed of 200 mm/min. Fig. 3 shows the stress–strain curve for the zone-drawn fibers before and after the zone annealing. Note that at around 2.5% of the elongation, there is a yielding point observed in both the fibers. Table 2 illustrates the tensile properties of the zone-drawn fibers before and after continuous zone-annealing experiments. It is interesting to find that after this continuous zone annealing the fibers exhibit a 2-fold increase in the elongation-at-break, a 16% decrease in the tensile modulus while their tensile strength is only marginally affected.

3.2. Ordered fiber structural evolution in zone-drawing and zone-annealing processes

Fig. 4a–c shows the three WAXD fiber patterns for the as-spun, after zone-drawn and zone-annealed fibers, respectively. It is interesting to observe that in Fig. 4a the as-spun WAXD fiber pattern shows the

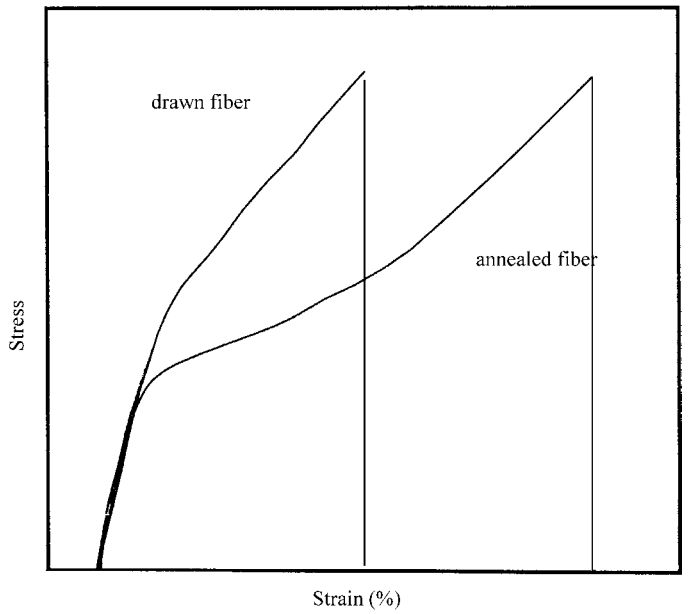

Fig. 3. Two stress–strain curves of the zone-drawn fibers before and after zone-annealing process.

Table 2
The mechanical properties of zone-drawn and zone-annealed fibers

Samples	Diameters (μm)	Tensile strength (GPa)	Elongation-at-break (%)	Modulus (GPa)
4.2× fibers zone-drawn	59	0.32	11	7.7
4.2× fibers zone-annealed	59	0.32	20	6.3
FS16 fibers	23	0.32	6.4	8.09
FS16 fibers zone-annealed	23	0.31	15	8.1

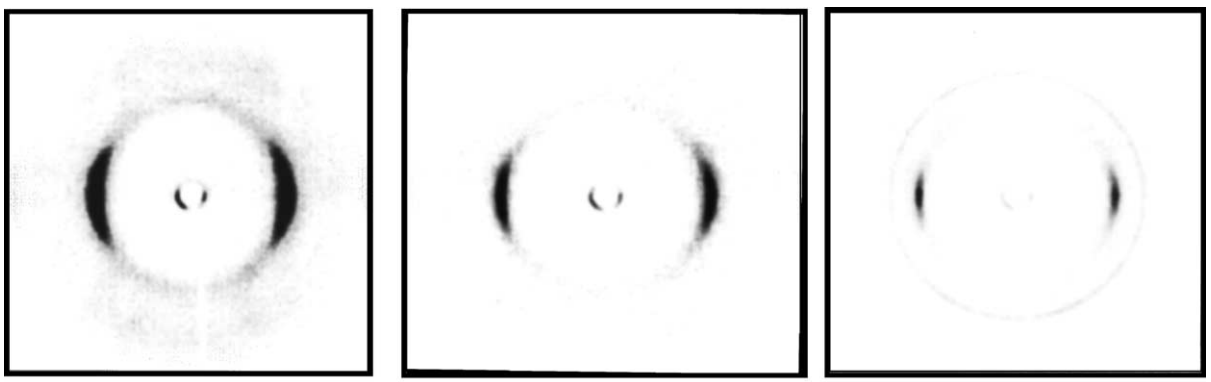

Fig. 4. Three WAXD patterns of the (a) as-spun, (b) zone-drawn and (c) zone-annealed fibers.

diffuse and weak (1 1 0) diffraction arcs, which corresponds to a relatively low crystallinity (20%) and a low degree of (1 1 0) crystal orientation (0.40). The apparent crystallite size along the [1 1 0] direction is 3.9 nm. For the 4.2× zone-drawn fibers in Fig. 4b, the WAXD pattern exhibit the improved (1 1 0) diffraction arcs, and its crystallinity increases to 32%, while the degree of (1 1 0) crystal orientation reaches 0.63. The apparent crystallite size along the [1 1 0] direction also increases slightly to 5.9 nm. Fig. 4c displays the WAXD pattern of the zone-annealed FS16 fibers. A short zone-annealing time of a few seconds leads an increase in crystallinity to 44% and the apparent crystallite size along the [1 1 0] direction is significantly increased to 8.0 nm. The degree of (1 1 0) crystal orientation is almost unaffected in the zone-annealing process. It also appears that after annealing the surface texture of the fibers becomes smoother. These results indicate that zone annealing can preserve the tenacity of the zone-drawn fiber yet, substantially improve the elongation-at-break.

Based on the WAXD results, the crystallinity, the degree of (1 1 0) crystal orientation and the apparent crystallite size along the [1 1 0] direction for different fibers are summarized in Table 3. The fibers produced by the conventional drawing process (FS22) exhibits a degree of crystallinity of 30%, a high degree of (1 1 0) crystal orientation (0.72) and an apparent crystallite size along the [1 1 0] direction of 8.1 nm [15]. After zone drawing and annealing, the 4.2× fibers show an increase in the crystallinity (37%) and a high degree of (1 1 0) orientation (0.63) when compared with the as-spun fibers. The apparent crystallite size along the [1 1 0] direction decreases to 5.9 nm after the zone-drawing and recovers to 7.0 nm after the zone-annealing.

Furthermore, it is interesting to compare two groups of samples, the zone-drawn 4.2× fibers and the FS16 fibers before and after zone-annealing process (Table 3). After the zone annealing, both the crystallinity, the apparent crystallite size along the [1 1 0] direction increase compared with their own precursor fibers (the zone-drawn fibers and the FS16 fibers, respectively). However, for the (1 1 0) crystal orientation after the zone annealing, both fibers are unchanged compared to the zone-drawn fibers. This indicates that the zone-annealing process is largely effective to further enhance crystal growth and perfect the crystals. This annealing process also relaxes internal stresses frozen in during the zone-drawing process and substantially increases the elongation-at-break.

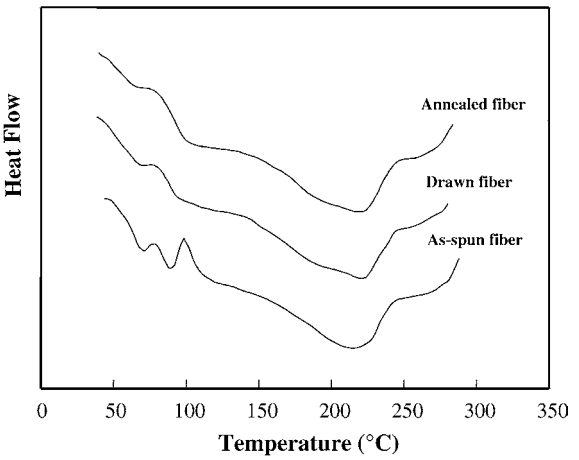

Fig. 5. Three DSC curves of the as-spun, zone-drawn and zone-annealed fibers.

3.3. Thermal properties and relaxation behaviors

Three DSC thermal diagrams for the as-spun, zone-drawn and zone-annealed fibers are shown in Fig. 5. For the as-spun fibers, an increase in heat

Table 3
The structure of the fibers before and after zone annealing

Samples	Crystallinity (%)	Crystal orientation [1 1 0]	Apparent crystallite size (nm)
As-spun fibers	20	0.40	3.9
FS22 fibers	30	0.72	8.1
4.2× fibers zone-drawn	28	0.63	5.9
4.2× fibers zone-annealed	37	0.63	7.0
FS16 fibers	32	0.67	6.8
FS16 fibers zone-annealed	44	0.68	8.0

capacity can be found at about 85 °C, which corresponds to the glass transition temperature (T_g), an exothermic transition at 100 °C caused by the crystallization, and an endothermic process at 215 °C for the crystal melting. The zone-drawn fibers exhibit a higher temperature T_g of about 92 °C due to the limitation of molecular motion caused by existence of the crystals [16,17] and molecular orientation. A melting endotherm at 222 °C is attributed to the crystal melting. No crystallization process can be seen during heating for the zone-drawn fibers, indicating that the crystallization is completed after this drawing process. The zone-annealed fibers show similar thermal behavior as the zone-drawn fibers.

The thermal shrinkage of the zone-drawn fibers before and after the zone annealing is displayed in Fig. 6. It can be observed that the zone-drawn fibers start shrinkage at a lower temperature (75 °C) in comparison to the zone-annealed fiber (90 °C). This is due to the fact that the internal stress frozen in the amorphous region decreases the T_g [18,19] and the amount of crystals in the zone-drawn fibers are not enough to hold on the relaxation of the oriented amorphous

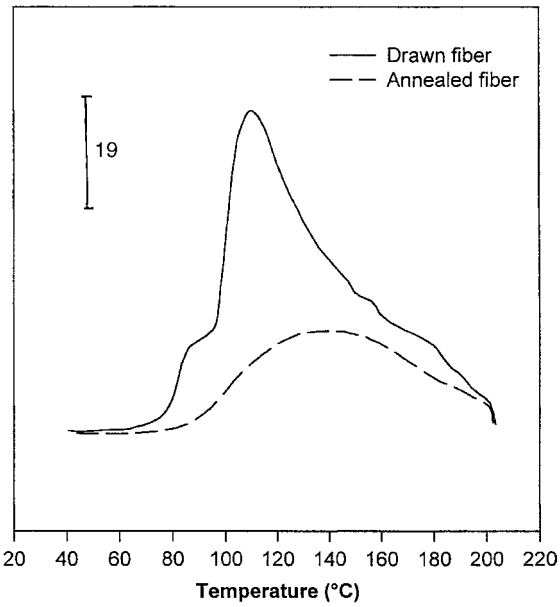

Fig. 7. The thermal shrinkage force of the drawn fibers before and after zone-annealing process.

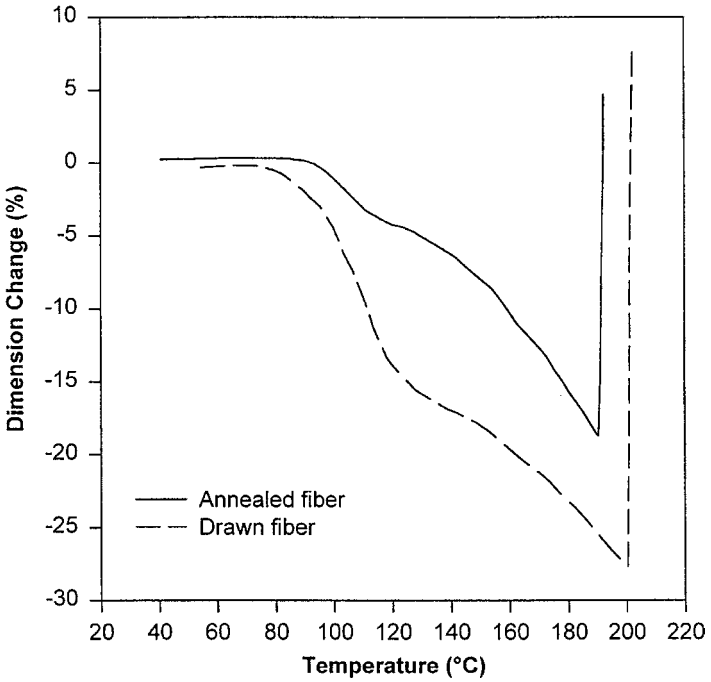

Fig. 6. The thermal shrinkage behavior of the zone-drawn fibers before and after zone-annealing process.

region. In addition, the shrinkage of the zone-drawn fibers is greater than that of the zone-annealed fibers. The thermal shrinkage force of the zone-drawn fibers before and after zone annealing is depicted in Fig. 7. It is evident that for the zone-drawn fibers the thermal shrinkage force starts at 75 °C and reaches a maximum at 110 °C. This corresponds to a maximum shrinkage occurring at 108 °C for zone-drawn fibers (Fig. 6). On the other hand, the zone-annealed fibers exhibit much mild shrinkage force, indicating that most of the stress has been relaxed during the annealing process. The high crystallinity in the zone-annealed fibers also assists the fiber dimensionality.

The development of the thermal shrinkage or the thermal shrinkage force above the T_g must be associated with the entropy relaxation of stretched chain molecules in the oriented amorphous regions of the fibers and it is dependent upon the degree of orientation and entanglements in this region as well as the crystallinity. The WAXD measurements show only minor changes in crystallinity and crystal orientation after the zone-drawn fibers underwent the zone-annealing process. It is observed that after zone-annealing at 145 °C the elongation-at-break of the fibers increases significantly since at this temperature the chain disentanglement process may be enhanced [20]. This suggests that the internal stress induced by entanglements in the amorphous regions has at least partially released which influences the behaviors of the thermal shrinkage and thermal shrinkage force.

Figs. 8 and 9 show the temperature dependence of E', E'' and $\tan\delta$ for the zone-drawn and zone-annealed fibers. In Fig. 8, the E' values of the zone-drawn fibers show a sudden drop starting at around 70 °C, which is frequency dependent, and this corresponds to the T_g. On the other hand, the E'' values exhibit a maximum between 70 and 95 °C, indicating energy dissipation associated with the T_g. For the zone-annealed fibers in Fig. 9, the significant drop of the E' values

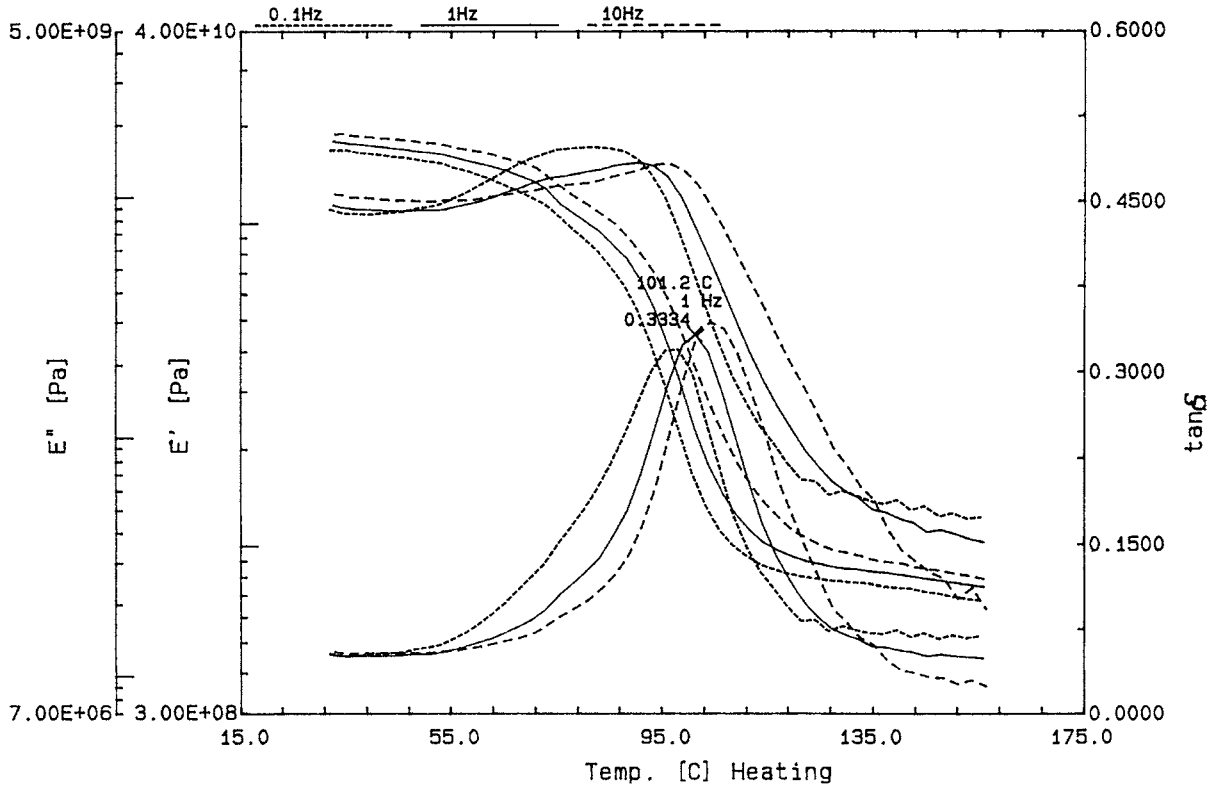

Fig. 8. The temperature dependence on the E', E'' and $\tan\delta$ of the zone-drawn fibers.

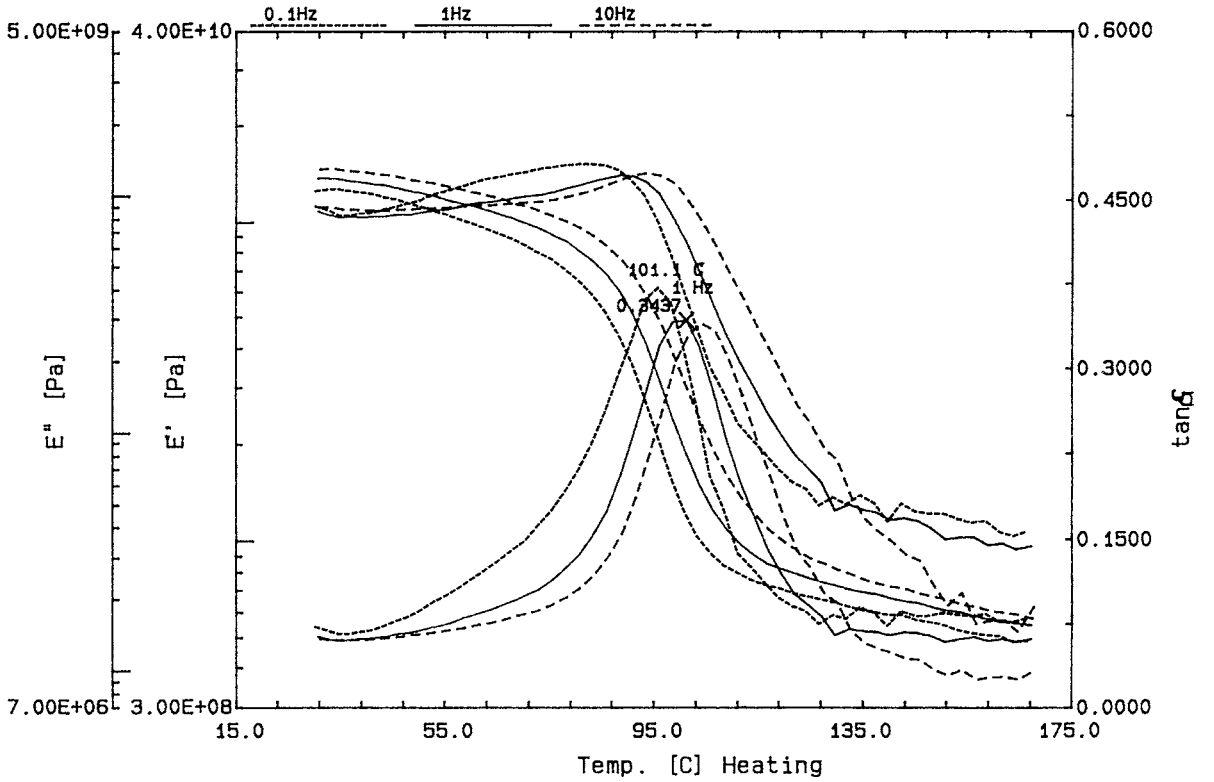

Fig. 9. The temperature dependence on the E', E'' and $\tan\delta$ of the zone-annealed fibers.

resulting from passing through the T_g is observed to shift to a higher temperature range. The modulus of zone-drawn fibers is higher than that of zone-annealed fibers. The activation energies (E_a) for both drawn and annealed fibers are calculated based on the logarithm of frequency versus reciprocal peak temperature of the $\tan\delta$. The E_a values are 837 and 538 kJ/mol for the zone-drawn and zone-annealed fibers, respectively. These results indicate that the zone-annealing process does relax internal stress which was frozen in during the drawing process.

4. Conclusion

The continuous zone-drawing and zone-annealing processes have been applied to AMLON^{TM} fibers to improve mechanical and thermal properties. Thermal analysis results show that the T_g of the fibers is between 85 and 92 °C, depending upon the orientation and crystallinity of the fibers. The crystal melting takes place in a broad temperature range peaked at around 220 °C. The thermal shrinkage behaviors reveal that zone-annealed fibers exhibit substantially improved fiber dimension stability. Mechanical measurements show that the tensile modulus and tensile strength of the as-spun fibers are 4 and 0.1 GPa, respectively. After continuous zone-drawing process, they increase to 10 and 0.3 GPa, correspondingly. The elongation-at-break of the 4.2× drawn fibers is 11%. After continuous zone-annealing process the tensile strength is unchanged, while the tensile modulus slightly decreases. However, the elongation-at-break increases up to 20% possibly due to the release of chain entanglements in the oriented amorphous region. The WAXD results show that after zone-drawing and zone-annealing the crystallinity, the apparent crystallite size along the [1 1 0] direction, and the degree of (1 1 0) crystal orientation increase in comparison to the as-spun fibers. However, the crystallinity and the

degree of (1 1 0) crystal orientation in the fibers show no apparent change between the zone-drawn fibers and zone-annealed fibers, yet the apparent crystallite size along the [1 1 0] direction exhibits significant increase due to the zone-annealing process. These results indicate that the annealing process is mainly responsible to the improvement of the amorphous structure and perfection of the crystals.

Acknowledgements

This work was supported by British Petroleum Company.

References

[1] H. Shiota, R. Nishida, T. Kida, N. Kohara, Y. Watanable, R. Kasahara, US Patent 5681512 A 971028, 1997.
[2] B.G. Min, T.W. Son, B.C. Kim, W.H. Jo, Polym. J. (Japan) 24 (1992) 841.
[3] BASF AG, Adv. Mater. (Newsletters) 15 (9) (1993) 4.
[4] T. Kunugi, A. Suzuki, M. Hashimoto, J. Appl. Polym. Sci. 26 (1981) 1951.
[5] T. Kunugi, J. Polym. Sci. Polym. Lett. Ed. 20 (1982) 329.
[6] T. Kunugi, T. Ito, M. Hashimoto, J. Appl. Polym. Sci. 28 (1983) 1951.
[7] T. Kunugi, I. Akiyama, M. Hashimoto, Polymer 23 (1982) 1199.
[8] T. Kunugi, A. Suzuki, E. Kubota, Koubunshi Ronbunsyu 49 (1992) 161.
[9] A. Suzuki, S. Maruyama, T. Kunugi, Konbunshi Ronbunsyu 49 (1992) 741.
[10] S.Z.D. Cheng, Z.-Q. Wu, M. Eashoo, S.L.C. Hsu, F.W. Harris, Polymer 32 (1991) 1803.
[11] M. Eashoo, Z.-Q. Wu, A.Q. Zhang, D.X. Shen, C. Tse, F.W. Harris, S.Z.D. Cheng, K.H. Gardner, B.S. Hsiao, Macromol. Chem. Phys. 195 (1994) 2207.
[12] D.X. Shen, Z.-Q. Wu, J. Liu, L.X. Wang, S.K. Lee, K.W. Harris, S.Z.D. Cheng, Polym. Polym. Compos. 2 (1994) 149.
[13] A. Suzuki, Y. Sato, T. Kunugi, J. Polym. Sci. Polym. Phys. Ed. 36 (1998) 473.
[14] R.C. Smierciak, E. Wardlow Jr., L.E. Ball, US Patent 5,618,901 (1997).
[15] J.A. Dacidson, H.-T. Jung, S.D. Hudson, S. Percec, Polymer 41 (2000) 3357.
[16] S.Z.D. Cheng, M.-Y. Cao, B. Wunderlich, Macromolecules 19 (1986) 1868.
[17] S.Z.D. Cheng, Z.-Q. Wu, B. Wunderlich, Macromolecules 20 (1987) 2802.
[18] F.E. Arnold Jr., D.X. Shen, C.J. Lee, F.W. Harris, S.Z.D. Cheng, H.W. Starkweather Jr., J. Mater. Chem. 3 (1993) 183.
[19] F.E. Arnold Jr., D.X. Shen, C.J. Lee, F.W. Harris, S.Z.D. Cheng, S.-F. Lau, J. Mater. Chem. 3 (1993) 353.
[20] B.J. Qian, Z.-Q. Wu, P.P. Hu, J. Qin, C.X. Wu, J.X. Zhao, J. Appl. Polym. Sci. 47 (1993) 1881.